A R C H I V E O F M E C H A N I C A L E N G I N E E R I N G

Volume 68 2021 Number 3

DOI: 10.24425/ame.2021.137050

Key words: cycloidal gearbox, dynamics, resonance, gearbox vibration, multibody dynamics, multibody simulation, finite element method, gearbox resonance

Roman Król [1]

Resonance phenomenon in the single stage cycloidal gearbox. Analysis of vibrations at the output shaft as a function of the external sleeves stiffness

In this paper a versatile analysis of the cycloidal gearbox vibrations and the resonance phenomenon was performed. The objective of this work was to show resonance phenomenon and vibrations study in the multibody dynamics model and in the finite element model of the cycloidal gearbox. The output torque was analyzed as a function of the external sleeves stiffness.

The results from the multibody dynamics model were verified in the finite element model using natural frequency with load stiffening, direct frequency response and direct transient response analyses.

It was shown that natural frequencies of the cycloidal gearbox undergo changes during motion of the mechanism. The gearbox passes through the thresholds of the increased vibration amplitudes, which lead to excessive wear of the external sleeves.

The analysis in the multibody dynamics model showed, that the increase in the external sleeves stiffness increases frequency of the second-order fluctuation at the output shaft. Small stiffness of the external sleeves guarantees lower frequency of the second order vibrations and higher peak-to-peak values of the output torque.

The performed research plays important role in the cycloidal gearbox design. This work shows gearbox dynamics problems which are associated with wear of the external sleeves.

1. Current research in cycloidal gearbox dynamics

There are many kinds of constructions of planetary gears. One of them are cycloidal gearboxes. The exemplary applications of these mechanisms are winches of the off-road vehicles or rescue helicopters. The main advantage of a cycloidal

✉ Roman Król, e-mail: r.krol@uthrad.pl

[1] Kazimierz Pulaski University of Technology and Humanities in Radom, Faculty of Mechanical Engineering, Poland. ORCID: 0000-0002-6279-9562

gearbox is the ability to work in high-loading conditions, when dimensions of a gearbox are relatively small. The disadvantage of these mechanisms are high vibrations at the output shaft. The vibration problem in cycloidal gearboxes is comprehensively studied in this paper.

Contemporary works in the field of cycloidal gearbox engineering are concerned with a range of topics, ranging from strength to dynamic analysis. Cycloidal gears are described by nonlinear, parametric functions, which make the kinematic and the dynamic analysis complex.

To perform a modal analysis, simplified models [1, 2] can be applied, where interactions between parts are modeled by springs and dampers.

In work [3], elastic torsional compliance of the internal pins was analyzed. Interesting remarks in that article include consideration of the internal sleeves as a shock absorber. The authors of the mentioned work stated that vibrations are one of the important problems in the cycloidal gearbox design. According to [3], backlash in the gear setup forms barriers in the dynamic model synthesis. The article also confirms that Finite Element Analysis is useful for determining stiffness and inertia properties of the gearbox parts.

The works [4] and [5] present kinematic analysis of the cycloidal gearbox. There is an incorrect conclusion in [5], where it is stated that the torque fluctuation at the input shaft does not significantly influence output. In the current article, it will be shown that torque fluctuation at the output shaft is close to the result of the input torque fluctuation multiplied by the gear ratio (Fig. 13).

There are some research papers, which undertake the problem of backlash in cycloidal gearboxes. The analysis of kinematic error and the tolerance of the design were undertaken in [6] and the analysis of contact was mentioned in [7].

The aim of [6] was to analyze the kinematic errors to reduce manufacturing cost, which can also be reduced by minimization of volume using a genetic algorithm [8] or gradient optimization methods [9, 10].

In works [7, 11] the contact was analyzed in the cycloidal gearbox models. Modelling of the contact in the cycloidal gearbox is an advanced topic in the mechanical systems simulation. There one should use appropriate algorithms because of difficult shape of cycloidal gears. The simple algorithms, like separation axis theorem, can be used only for convex polygons, while the cycloidal gear is often represented as a concave polygon. Due to the difficulties in programming precise simulation models with contact and multibody motion analysis, the use of advanced engineering software packages and experimental verification of the cycloidal gearbox vibrations is required.

In works [12–14], vibration analysis of gearboxes was performed. There is a high number of works concerned with fault detection [15–26], which also involves analysis of vibration. The review of these methods can be found in [23].

The fluctuation in the input torque comes from the input engine. The influence of the motor current [27] on the torques in the gearboxes is rarely considered in

technical literature. Some works deal with identification of the vibrations signatures [28] and the angular position of the gear [29].

In the present article, the problem of resonance phenomenon is shown in the theoretical models of a cycloidal gearbox with reduced stiffnesses of the external sleeves. To invoke the resonance state in the real gearbox, the input torque with high frequency should be used. High frequencies in a transient analysis demand large data storage and long computational time. In the analyses described in this article, reduced stiffness of the external sleeves made it possible to show the output torque with gradually increased vibration amplitude.

This study shows important an issue in a cycloidal gearbox construction, which concerns passing through the thresholds of vibrations with high amplitudes. Natural frequencies of a gearbox undergo changes with the motion of the mechanism and various frequency components of the input torque can be equal to the natural frequencies for the given position of the gears. Stable work of the gearbox is shown in Fig. 9 and an unfavorable work with high amplitudes is shown in Fig. 8. Both figures present time courses of the output torque for the excitation with disparate frequencies.

The vibrations of the torque at the output shaft are also analyzed as a function of the external sleeves stiffness, which leads to the interesting conclusions concerning peak-to-peak values of the output torque and its second-order oscillations. The aim of the presented analyses is to show the cycloidal gearbox construction problems, which should be considered during the design process.

The analysis presented in the current article was performed in the Multibody Dynamics Model (MDM) and verified in the Finite Element Model (FEM). In the FEM, the approach similar to [2] was applied. Springs were used for the simulation of the bending stiffness and the rigid body links were utilized to transfer contact forces from the cycloidal gears to the external sleeves. In the MDM and FEM, the friction and the structural damping were neglected. The FEM contains no viscous damping components. Contact damping between parts of MDM was set to 10^{-3} Ns/m.

In the MDM, compliance of the internal sleeves was modeled using bushings (the bearings with the radial stiffness component). The results of the multibody analysis showed that, in the resonance, high radial displacements of the internal sleeves occur. This method of modelling stiffness corresponds to the bending of these sleeves in the real mechanism. In this work, compliance of the external sleeves was also included in the MDM, resulting with higher output torque values for the more compliant sleeves.

Both models (the FEM and the MDM) were built without any specified backlash related to the position of the external sleeves. The spline fit accuracy for the geometry designed in the Autodesk Inventor was set to 0.00001 m. The influence of backlash on the dynamics of the cycloidal gearbox can be studied in further research using the MDM presented in this article.

This paper shows vibration analysis methods using the multibody analysis or the natural frequency analysis in the MDM and prestress normal modes, direct transient response or direct frequency response analysis in the FEM. The main drawback of the presented analyses is the simulation of the sleeves bending using an equivalent radial stiffness. The analysis of the FEM is very time consuming, hence joining static or nonlinear structural analysis with the multibody dynamics analysis leads to very long analysis times. In this problem, solutions are divided into specialized groups. The analysis can determine stresses in quasi-static models or one can apply multibody dynamics analysis, which uses rigid bodies. In the MSC Adams software, bushings can be used as a kind of bearings with radial stiffness, which provide compliance of the parts during the motion of the mechanism. It is also possible to perform natural frequency analysis in the MSC Adams. This analysis can be compared with the direct frequency response analysis in the FEM. One of the solved natural frequencies can be included in the input torque, which should invoke resonance in the MDM. In this paper, output torque oscillations in the resonance are shown (Fig. 6), after application of the prepared input torque with one of the natural frequencies. The analysis of the resonance is important because the experimental research [30, 31] showed that wear of the sleeves is caused by the excessive vibrations. In future research, it would be worth analyzing the effect of motor current on the torque fluctuation at the input shaft.

2. The multibody dynamics model (MSC Adams)

The geometry of cycloidal gearbox was prepared in Autodesk Inventor. The advantage of the mentioned 3D modelling software is the possibility of verifying collision between parts of the MDM. Cycloidal gears should be aligned to the specific starting position, in which there are no interferences between parts.

Application of bushings and bearings in the MDM makes possible motion of the kinematic chains. These standard rotational joints in MSC Adams connect specified points of the parts and allow for relative rotational motions between the ground and the external sleeves, the internal pins and the internal sleeves, the input shaft and the cycloidal wheels or the ground and the shafts.

Bushings have radial stiffness, which was determined in the separate static analysis for each part in the Autodesk Nastran In-CAD. The radial stiffnesses of the bushings are equal to the three-point bending stiffnesses of the corresponding part (external sleeves, internal sleeves and input shaft).

The assembly of the single-stage cycloidal gearbox designed in MSC Adams is shown in Fig. 1. The values of the radial stiffnesses in bushings are given in Table 1 and the schematic is shown in Fig. 2. In the schematic, linear springs represent radial stiffnesses of the bushings or the bearings without the compliance ($k = \infty$).

The spring $k_1 = \infty$ is set as the rigid bearing at the input shaft, $k_2 = \infty$ is the rigid bearing at the output shaft and $k_5 = \infty$ is the rigid bearing between the shafts. Radial stiffnesses are present in the bushings k_3, k_4, k_6 and k_7. The radial stiffness

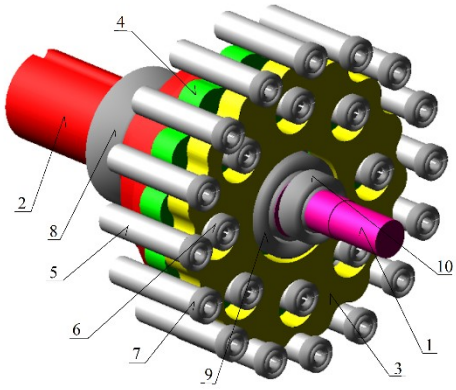

Fig. 1. The MDM in MSC Adams. Input shaft (1), output shaft (2), external cycloidal gear (3), internal cycloidal gear (4), external sleeve (5), bushing at the internal sleeve (6), bushing at the external sleeve (7), rigid bearing at the output shaft (8), bushing between the external cycloidal gear and the input shaft (9), rigid bearing at the input shaft (10)

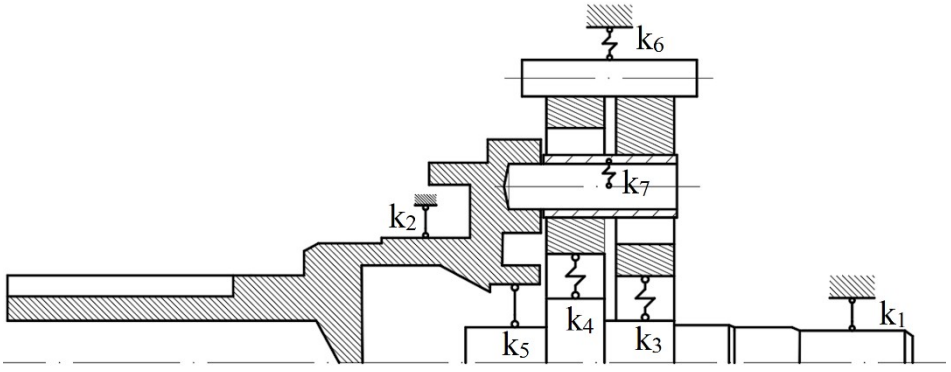

Fig. 2. Radial stiffnesses in the bushings (k_3, k_4, k_6, k_7) and the rigid bearings (k_1, k_2, k_5). The values of the stiffnesses are given in Table 1

Table 1.
Radial stiffnesses in the bushings, which correspond to the three-point bending stiffness of the given part

Part	Housing	Stiffness symbol (Fig. 2)	Radial stiffness [N/m]
External sleeve	ground	k_6	300 000 (analysis dependent)
Internal pin	Internal sleeve	k_7	12 000 600
Input shaft	External cycloidal gear	k_3	3 723 978 700
Input shaft	Internal cycloidal gear	k_4	3 135 975 900
Input shaft	Output shaft	$k_5 = \infty$	rigid
Output shaft	ground	$k_2 = \infty$	rigid
Input shaft	ground	$k_1 = \infty$	rigid

k_7 is applied in the bushings between the internal pins and the internal sleeves, which can rotate around the first ones to reduce friction between the cycloidal gears and the pins. Table 1 contains exemplary stiffness for the external sleeves. There are given different values dependent on the analysis presented in this article.

3. The finite element model (Autodesk Nastran In-CAD)

Two variations of the FEM were designed in the Autodesk Nastran In-CAD. In the first FEM (Fig. 3a, Fig. 4a) contact forces are transferred from the cycloidal wheel to the external sleeves through the rigid body links (red color). The rigid body links intersect in the instantaneous center of rotation of each of the cycloidal

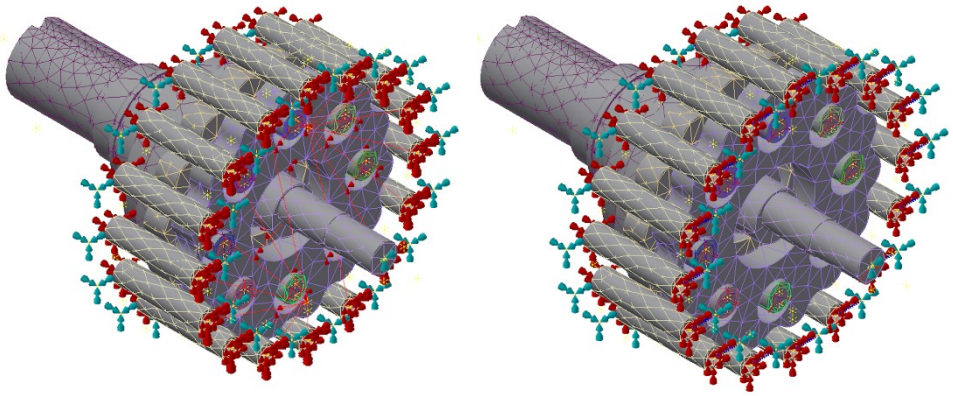

(a) with rigid body links

(b) with contacts defined instead of rigid body links

Fig. 3. The finite element model. The mesh is coarse

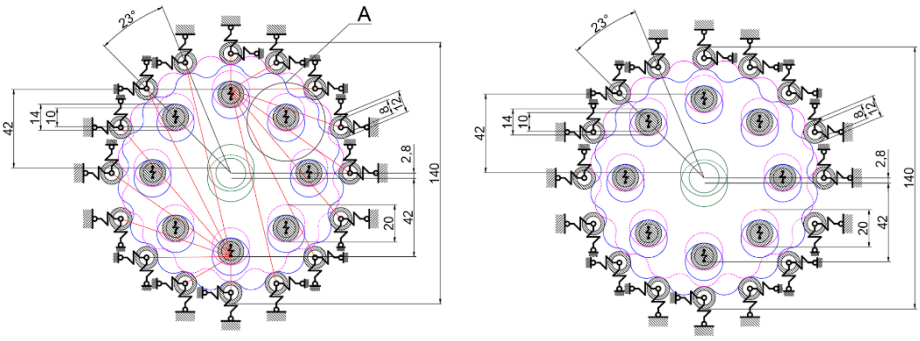

(a) with the rigid body links (red) and springs, whose stiffness is equivalent to the three-point bending stiffness of the external and internal sleeves

(b) with the contacts defined instead of rigid body links

Fig. 4. Schematic of the FEM. The dimensions are in mm

gears. In the second FEM (Fig. 3b, Fig. 4b), rigid body links were removed and the contact between the parts of the cycloidal gearbox was set.

The surface contact between the eccentric parts of the input shaft and the cycloidal gears was set up with the offset of 0.012 m. The Young's modulus of the external sleeves in both FEMs was set to the high value $E = 1 \cdot 10^{11}$ MPa.

In both FEMs, rigid body links are placed at each external sleeve, connecting boundary nodes at the sleeve edge with the center point. Springs which simulate three-point bending stiffness of the external sleeve are placed at these points. The other end of the spring is fixed. The external sleeve can rotate around its axis of symmetry.

The springs are also placed between the internal pins and the internal sleeves, but the method of connection is more complicated (Fig. 5). In the real model, internal pins are mounted in the output shaft and the hollow internal sleeves are placed on the pins as bearings. The purpose of the internal sleeves is to reduce friction between the internal pin and the cycloidal gear. The rigid body links connect outer edge of the internal sleeve with one end of the spring and the outer edge of the internal pin with the other end of spring. Additionally, the rigid body links which create the web for the hole of the cycloidal gear are connected with the center point of the rigid body links that create the web for the internal sleeve. This connection establishes contact between the cycloidal gear and the internal sleeve, which in the second FEM is substituted by the separation contact.

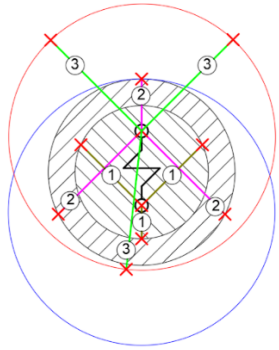

Fig. 5. The detail "A" from Fig. 4a. The scheme of the connection between the spring and the rigid body links: in the internal pin (1), in the internal sleeve (2) and in the hole of the cycloidal gear (3)

4. Resonance in the cycloidal gearbox

Cycloidal gearboxes have a very stiff structure. The input shaft, external and internal sleeves are short, the output shaft is very massive and the cycloidal gears are very stiff discs. Due to their very stiff construction, cycloidal gearboxes have high values of natural frequencies. The aim of this article is to determine natural

frequencies of the external sleeves and invoke a resonance in the multibody analysis by the application of the prepared sine input torque. The input torque should contain the frequency, which was determined in the modal analysis.

In the MDM with external sleeves of stiffness set to 300 000 N/m, the natural frequency analysis was performed. On the basis of that analysis, the natural frequency $f = 556.8$ Hz was determined, which corresponds to the bending mode of the external sleeves. The prepared sine input torque with the same frequency, constant component $c = 1.5$ Nm and amplitude $A = 0.1$ Nm was applied at the input shaft in the multibody analysis. The settings of the analysis were $n = 3341$ steps and the analysis time was $t = 0.24$ s. Vibration amplitude of the internal and external sleeves gradually increased and the gearbox mechanism was locked up after 0.2287 s of analysis.

In the MSC Adams, the state variables and the request were programmed to solve the output torque on the basis of the forces acting on the internal sleeves and the sleeves' displacements. The output torque in the multibody analysis is shown in Fig. 6 as the response on the mentioned above sine input torque with $f = 556.8$ Hz. The angle of the internal sleeve rotation for the same analysis is shown in Fig. 7.

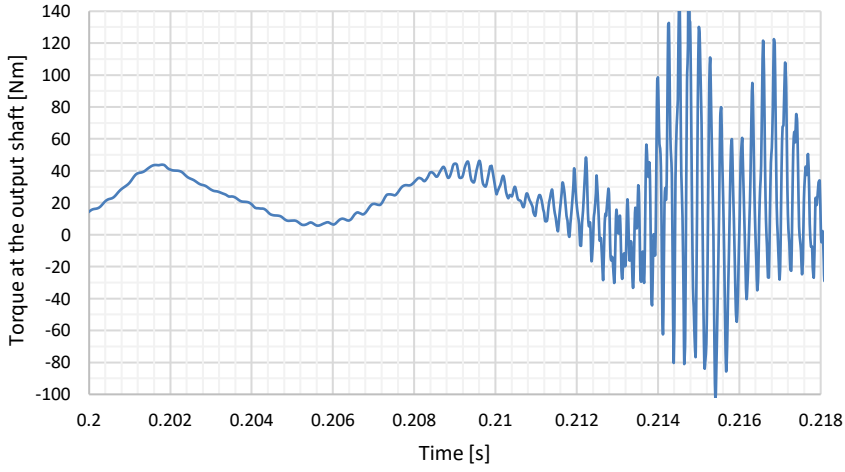

Fig. 6. The resonance in the cycloidal gearbox. The input torque frequency is 556.8 Hz, the constant component is 1.5 Nm and the amplitude is 0.1 Nm

In the MDM, the natural frequency analysis was also performed for various positions of the cycloidal gears. For each position of the cycloidal gears, disparate natural modes was obtained. The dynamical characteristics of the cycloidal gearbox change during its movement. It is difficult to predict which frequency components of the input torque will cause significant vibration amplitudes or the resonance state. The natural frequency analysis in the initial position of gearbox showed two frequencies: 8.87 Hz and 10.74 Hz, which are close to the excitation frequency in the experimental stand [32], when the cycloidal gearbox worked with

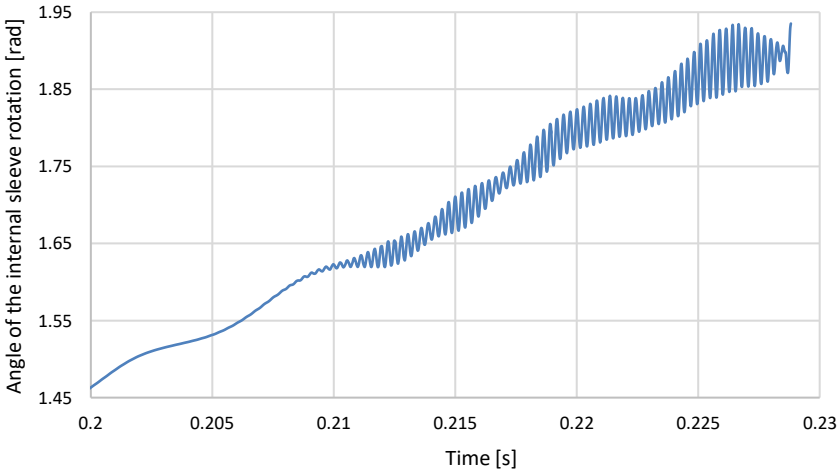

Fig. 7. The resonance in the cycloidal gearbox. The angle of the internal sleeve rotation for the input torque with the frequency 556.8 Hz, the constant component 1.5 Nm and the amplitude 0.1 Nm

the speeds close to 500 RPM (8.33 Hz). For each analyzed position of the cycloidal gears, there were the same natural modes of the external sleeves bending. These natural frequencies were 556.8 Hz for the stiffness of the external sleeves set to 300 000 N/m and 3594.3 Hz for the 250 000 000 N/m.

Some frequencies of the input torque can cause the work with a high output torque amplitudes (Fig. 8). There are also frequencies, for which the gain of the amplitude is not higher than the gear ratio (Fig. 9).

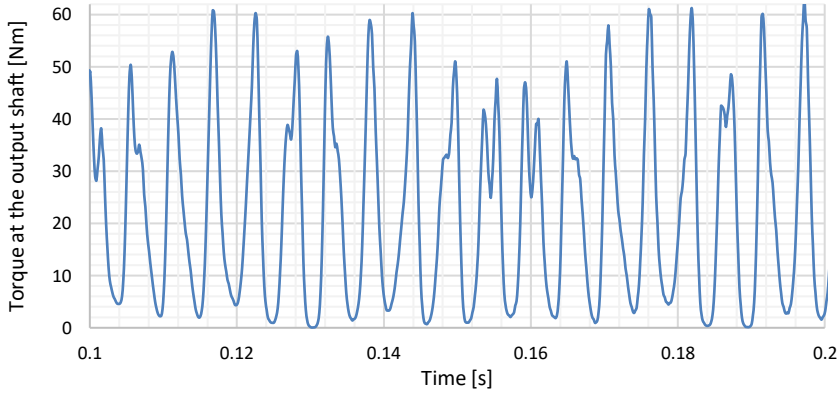

Fig. 8. Torque at the output shaft for the excitation with the sine input torque. The frequency of the input torque is 12 Hz, the constant component is 1.5 Nm and the amplitude is 0.1 Nm

In the MDM, the input torque measured in the experimental stand [32] was applied to the input shaft. The measured input torque with fluctuation is shown in Fig. 10. In Figs 13–15, one can see significant gain of the input torque fluc-

tuation during stable work of the cycloidal gearbox. The output torque vibrations significantly depend on the stiffness of the gearbox parts.

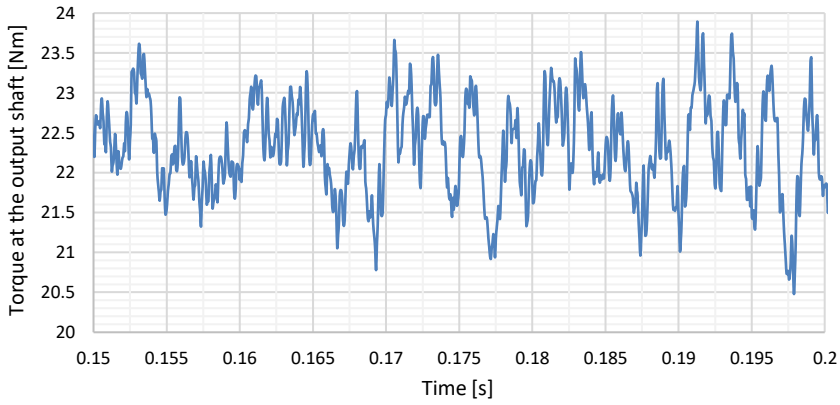

Fig. 9. Torque at the output shaft for the excitation with the sine input torque. The frequency of the input torque is 100 Hz, the constant component is 1.5 Nm and the amplitude is 0.1 Nm

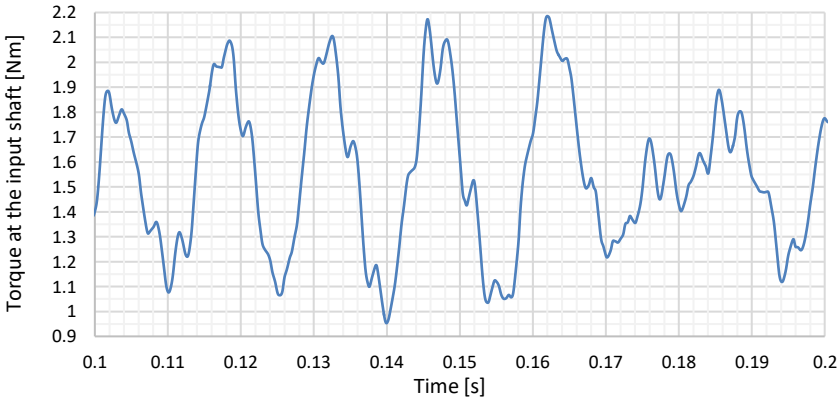

Fig. 10. The input torque with fluctuation measured in the measurement stand

4.1. Natural frequency analysis with load stiffening

For the FEM, the natural frequency analysis with load stiffening was performed. The model of the cycloidal gearbox (Fig. 4a) was loaded by the constant input torque of 1.5 Nm and the constant equilibrating output torque of 22.5 Nm. The natural frequency analysis with load stiffening solves the initially set number of natural frequencies taking into account changes in stiffness due to external load.

The natural frequencies for the model with rigid body links (Fig. 4a) are presented in Table 2. The analysis for the model shown in Fig. 4b, in which rigid body links were substituted by the separation contacts, resulted only in rigid body motion with natural frequencies lower than 1 Hz.

Table 2.

Convergence of the natural frequencies for the cycloidal gearbox FEM shown in Fig. 4a

Number of finite elements in FEM	18057	19494	22600	35164	64438	169610	489049
Natural frequency with load stiffening [Hz]	286.99	286.51	285.61	281.31	283.05	282.55	281.72
Natural frequency without load stiffening [Hz]	287.08	286.57	285.68	281.39	283.12	282.61	281.78

4.2. Direct frequency response analysis

The direct frequency response analysis was performed for the FEM (Fig. 4b) without the rigid body links and with contact modelling. The aim of the analysis was to determine the maximum rotation and the maximum displacement in the model as a function of the input torque frequency. The frequency range was set to 1–800 Hz (Fig. 11). The maximum values of the rotation and displacement appear at the frequency 578.9 Hz. The maximum rotation is $8.32 \cdot 10^{-7}$ rad and the maximum displacement is $4.8 \cdot 10^{-8}$ m ($4.8 \cdot 10^{-5}$ mm). Changing the range to the values 578.5–579.5 Hz and setting the divisions to 300 frequencies one obtains the values of $6.596 \cdot 10^{-5}$ rad for the rotation magnitude and $3.82 \cdot 10^{-6}$ m ($3.82 \cdot 10^{-3}$ mm) for the displacement magnitude, which appear at 578.7 Hz. Maximum rotation and maximum displacement values appeared in one of the external sleeve nodes.

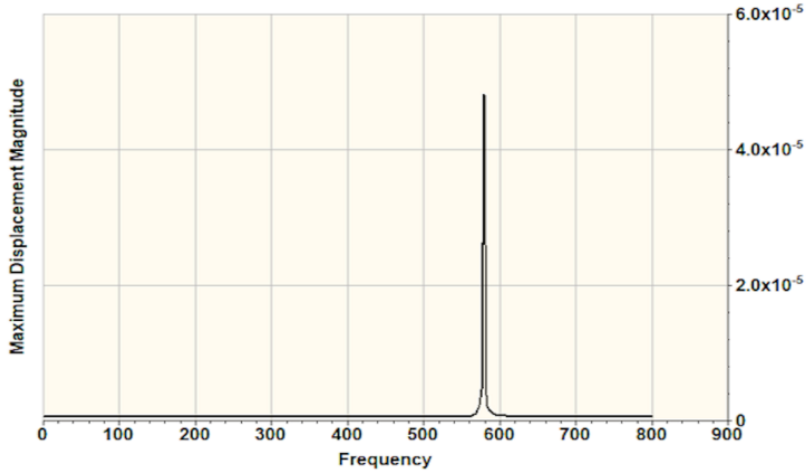

Fig. 11. The direct frequency response analysis in the FEM: maximum displacement magnitude [mm] versus frequency [Hz]

4.3. Direct transient response analysis

For the FEM with contact modelling (Fig. 4b), the direct transient response analysis was performed. The sine torque with frequency of 578.7 Hz, which was determined in the direct frequency response analysis, was applied at the input shaft. The constant component of the input torque was 1.5 Nm and the amplitude was 0.1 Nm. The time response is shown in Fig. 12.

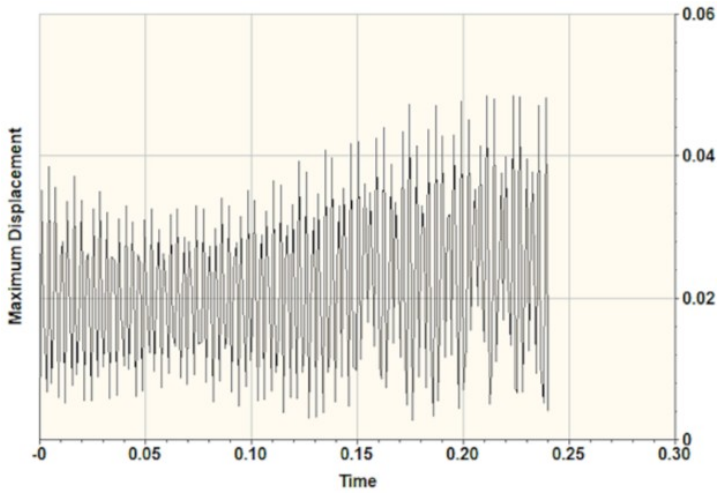

Fig. 12. The direct transient response analysis in the FEM with contact modeling: time course [s] of the maximum displacement [mm]

In the direct transient response analysis, the time step length is $\Delta t = 6.91443 \cdot 10^{-5}$ s, the number of time steps is $n = 3471$ and the analysis time is 0.24 s. In this analysis, despite many attempts to adjust the time increment, it was impossible to obtain as high vibration amplitude gain as that in the MDM (Fig. 6).

5. Influence of the external sleeve stiffness on the torque at the output shaft

The measured input torque with fluctuation (Fig. 10) was multiplied by the gear ratio and compared with the output torque obtained in the multibody analysis (Fig. 13). The analysis was performed without friction. The results show energy losses caused by contact modelling between cycloidal gearbox parts.

The analyses using the MDM was also performed for various stiffnesses of the external sleeves. The input torque measured in the experimental stand (Fig. 10) and the sine torque were applied in these analyses.

In the MDM, external sleeves are mounted on the bushings. Stiffness of these elements can be set to a random value. The multibody analysis was performed in the following two variants. First, the stiffness 300 000 N/m was set for each bushing

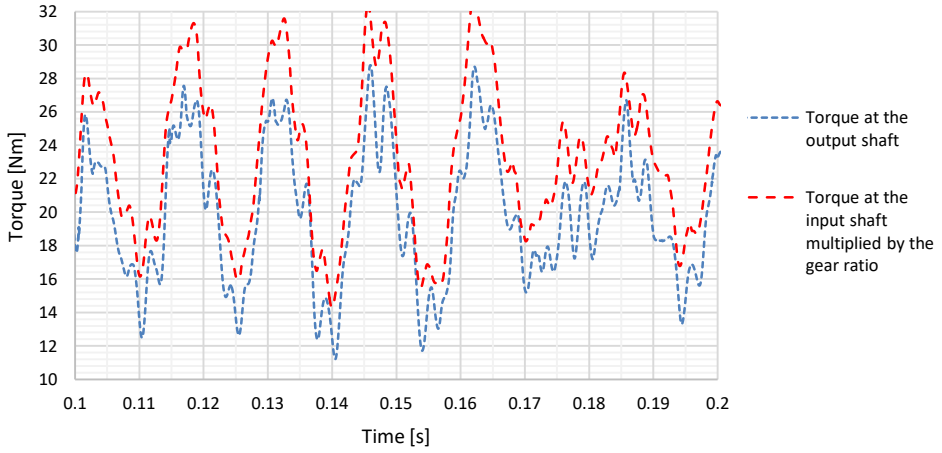

Fig. 13. Output torque in the MDM and the input torque with fluctuation multiplied by the gear ratio

in the external sleeves and then the analysis was repeated for 200 000 000 N/m. The torque at input shaft was set to the measured torque with fluctuation (Fig. 10). The output torque as a response to the mentioned input torque is shown in Fig. 14.

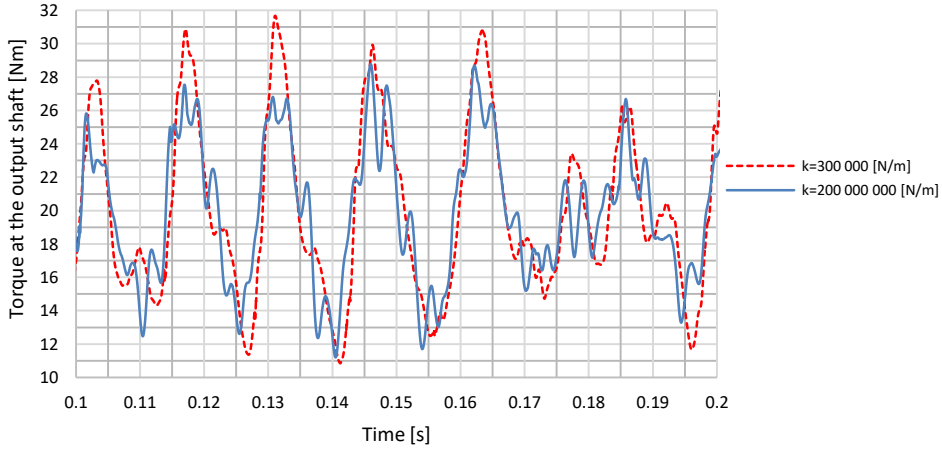

Fig. 14. Output torque for the various stiffnesses of the external sleeves. The input torque with fluctuation from measurement stand was applied at input shaft

Next, the multibody analysis was performed for the excitation with a sine torque. The frequency of the torque was 1 kHz, the amplitude 0.1 Nm and the constant component 1.5 Nm. The analysis was performed for the rigid model, where all bushings were substituted by the bearings and for two variants of stiffness of the external sleeves: 300 000 N/m and 200 000 000 N/m. The output torques for each variant are shown in Fig. 15.

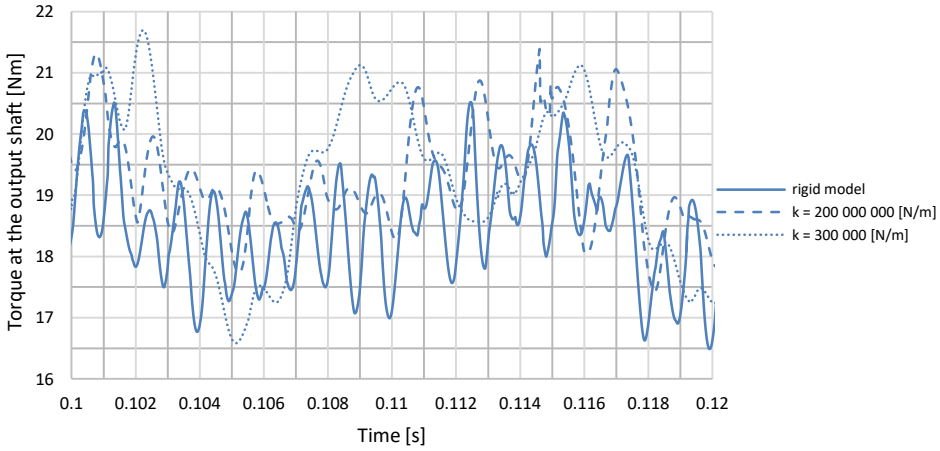

Fig. 15. Output torque for the various stiffnesses of the external sleeves. The frequency of the sine input torque is 1 kHz, amplitude is 0.1 Nm and constant component is 1.5 Nm

6. Conclusions

Cycloidal gearboxes have stiff structure, hence torques with high frequency components are needed to invoke the resonance state. The natural frequency of 556.8 Hz corresponds to the natural mode of the external sleeve bending, whose stiffness is 300 000 N/m. Increasing the stiffness to reflect the real state in the model causes an increase in the natural frequency. Setting the external sleeve bending stiffness to 250 000 000 N/m (the stiffness of the steel sleeve with the same geometry) increases the natural frequency to 3594.3 Hz. These values of excitation frequencies can be reached only in gearboxes with a high number of lobes and working with high input speeds.

In the gearbox design it is difficult to predict changes of the natural modes during motion of the gearbox mechanism. The modal analysis in the initial position showed two frequencies: 8.87 Hz and 10.74 Hz, which correspond to the modes other than external sleeves bending. The emergence of these modes can lead to thresholds of work with high vibration amplitudes, which can lead to an excessive wear of the external sleeves. This problem emerged during experimental research in the measurement stand presented in [32]. The output torque with increased amplitude is shown in Fig. 8 for the frequency of the sine input torque of 12 Hz (MDM).

The resonance in the MDM caused angular oscillations with 0.075 rad (4.3º) amplitude. Due to large angular deformations in the resonance, the output torque peak-to-peak value in the scope of analysis time is 240 Nm. It is over 10-times greater than the amplitude of the output torque during in stable work of the cycloidal gearbox.

In the FEM, rigid body links transfer forces from the cycloidal gear to the external sleeves. The length of the rigid body links should change with the motion of the cycloidal gearbox mechanism, and this model can be used only for modelling the instantaneous motion of the gearbox. In the prestress natural frequency analysis one of the natural frequencies is ≈281 Hz which is smaller than the value in the MDM (556.8 Hz with the corresponding mode shape). The conclusion is that modelling a cycloidal gearbox as the MDM without the rigid body links results in the stiffness of the elements higher than that for the FEM with bodies covered by the finite element mesh. The prestress state imposed by the application of the constant input and output torques does not influence the natural frequency in a meaningful way.

The direct frequency response analysis showed a peak at the frequency of 578.7 Hz in the maximum displacement diagram (Fig. 11). This value is close to the resonance frequency 556.8 Hz in the MDM. The FEM used in the direct frequency response analysis was built with contacts and without rigid body links. The use of models with rigid body links in the instantaneous static equilibrium gives inaccurate results when the dynamic analysis is considered. The differences between natural frequencies in the direct frequency response analysis for the FEM without rigid body links and in the MDM arise from different methods of modeling the stiffness. In the MDM all bodies are rigid and three-point bending stiffness is modeled using bushings. In the FEM the bodies are covered by the finite element mesh and deformations of these bodies are possible.

Despite many attempts of adjusting the value of time increments, there was no significant rise in displacement magnitude in the direct transient response analysis in the FEM (Fig. 12). It can be due to the contact modelling in Nastran In-CAD, where the default damping coefficient is too high.

The analysis in the MDM showed that the increase in the external sleeves stiffness increases frequency of the second order fluctuation at the output shaft (Fig. 14). Small stiffness of the external sleeves guarantees lower frequency of the second-order vibrations and higher peak-to-peak values of the output torque (Fig. 15).

Acknowledgements

This research utilised the MSC Software National Scientific Software License, operated by the TASK Computer Centre in Gdańsk (Poland). This license was funded by a computational grant obtained by Kazimierz Pulaski University of Technology and Humanities in Radom, Poland.

Manuscript received by Editorial Board, June 16, 2021;
final version, August 04, 2021.

References

[1] M.Blagojević, M. Matejić, and N. Kostić. Dynamic behaviour of a two-stage cycloidal speed reducer of a new design concept. *Technical Gazette*, 25(Supplement 2):291–298, 2018. doi: 10.17559/TV-20160530144431.

[2] M. Wikło, R. Król, K. Olejarczyk, and K. Kołodziejczyk. Output torque ripple for a cycloidal gear train. *Proceedings of the Institution of Mechanical Engineers, Part C: Journal of Mechanical Engineering Science*, 233(21–22):7270–7281, 2019. doi: 10.1177/0954406219841656.

[3] N. Kumar, V. Kosse, and A. Oloyede. A new method to estimate effective elastic torsional compliance of single-stage Cycloidal drives. *Mechanism and Machine Theory*, 105:185–198, 2016. doi: 10.1016/j.mechmachtheory.2016.06.023.

[4] C.-F. Hsieh. The effect on dynamics of using a new transmission design for eccentric speed reducers. *Mechanism and Machine Theory*, 80:1–16, 2014. doi: 10.1016/j.mechmachtheory.2014.04.020.

[5] R. Król. Kinematics and dynamics of the two stage cycloidal gearbox. *AUTOBUSY – Technika, Eksploatacja, Systemy Transportowe*, 19(6):523–527, 2018. doi: 10.24136/atest.2018.125.

[6] K-.S. Lin, K.-Y. Chan, and J.-J. Lee. Kinematic error analysis and tolerance allocation of cycloidal gear reducers. *Mechanism and Machine Theory*, 124:73–91, 2018. doi: 10.1016/j.mechmachtheory.2017.12.028.

[7] L.X. Xu, B.K. Chen, and C.Y. Li. Dynamic modelling and contact analysis of bearing-cycloid-pinwheel transmission mechanisms used in joint rotate vector reducers. *Mechanism and Machine Theory*, 137:432–458, 2019. doi: 10.1016/j.mechmachtheory.2019.03.035.

[8] A. Robison and A. Vacca. Multi-objective optimization of circular-toothed gerotors for kinematics and wear by genetic algorithm. *Mechanism and Machine Theory*, 128:150–168, 2018. doi: 10.1016/j.mechmachtheory.2018.05.011.

[9] R. Król, M. Wikło, K. Olejarczyk, K. Kołodziejczyk, and A. Zieja. Optimization of the one stage cycloidal gearbox as a non-linear least squares problem. In: T. Uhl (ed.) *Advances in Mechanism and Machine Science. Proceedings of the 15th IFToMM World Congress on Mechanism and Machine Science*, pages 1039–1048, Cracow, Poland, 15-18 July, 2019. doi: 10.1007/978-3-030-20131-9_103.

[10] R. Król. Updated software for the one stage cycloidal gearbox optimization (MATLAB scripts) (2.0). Zenodo, 2021. doi: 10.5281/zenodo.4737264.

[11] L.X. Xu and Y.H. Yang. Dynamic modeling and contact analysis of a cycloid-pin gear mechanism with a turning arm cylindrical roller bearing. *Mechanism and Machine Theory*, 104:327–349, 2016. doi: 10.1016/j.mechmachtheory.2016.06.018.

[12] M. Pfabe and C. Woernle. Reducing torsional vibrations by means of a kinematically driven flywheel – Theory and experiment. *Mechanism and Machine Theory*, 102:217–228, 2016. doi: 10.1016/j.mechmachtheory.2016.03.011.

[13] Y. Chen, X. Liang, and M.J. Zuo. Sparse time series modeling of the baseline vibration from a gearbox under time-varying speed condition. *Mechanical Systems and Signal Processing*, 134:106342, 2019. doi: 10.1016/j.ymssp.2019.106342.

[14] R. Yang, F. Li, Y. Zhou, and J. Xiang. Nonlinear dynamic analysis of a cycloidal ball planetary transmission considering tooth undercutting. *Mechanism and Machine Theory*, 145:103694, 2020. doi: 10.1016/j.mechmachtheory.2019.103694.

[15] W. He, B. Chen, N. Zeng, and Y. Zi. Sparsity-based signal extraction using dual Q-factors for gearbox fault detection. *ISA Transactions*, 79:147–160, 2018. doi: 10.1016/j.isatra.2018.05.009.

[16] D. Zhang and D. Yu. Multi-fault diagnosis of gearbox based on resonance-based signal sparse decomposition and comb filter. *Measurement*, 103:361–369, 2017. doi: 10.1016/j.measurement.2017.03.006.

[17] C.U. Mba, V. Makis, S. Marchesiello, A. Fasana, and L. Garibaldi. Condition monitoring and state classification of gearboxes using stochastic resonance and hidden Markov models. *Measurement*, 126:76–95, 2018. doi: 10.1016/j.measurement.2018.05.038.

[18] C. Wang, H. Li, J. Ou, R. Hu, S. Hu, and A. Liu. Identification of planetary gearbox weak compound fault based on parallel dual-parameter optimized resonance sparse decomposition and improved MOMEDA. *Measurement*, 165:108079, 2020. doi: 10.1016/j.measurement.2020.108079.

[19] W. Teng, X. Ding, H. Cheng, C. Han, Y. Liu, and H. Mu. Compound faults diagnosis and analysis for a wind turbine gearbox via a novel vibration model and empirical wavelet transform. *Renewable Energy*, 136:393–402, 2019. doi: 10.1016/j.renene.2018.12.094.

[20] Y. Lei, D. Han, J. Lin, and Z. He. Planetary gearbox fault diagnosis using an adaptive stochastic resonance method. *Mechanical Systems and Signal Processing*, 38(1):113–124, 2013. doi: 10.1016/j.ymssp.2012.06.021.

[21] L. Hong, Y. Qu, J.S. Dhupia, S. Sheng, Y. Tan, and Z. Zhou. A novel vibration-based fault diagnostic algorithm for gearboxes under speed fluctuations without rotational speed measurement. *Mechanical Systems and Signal Processing*, 94:14–32, 2017. doi: 10.1016/j.ymssp.2017.02.024.

[22] S. Schmidt, P.S. Heyns, and J.P. de Villiers. A novelty detection diagnostic methodology for gearboxes operating under fluctuating operating conditions using probabilistic techniques. *Mechanical Systems and Signal Processing*, 100:152–166, 2018. doi: 10.1016/j.ymssp. 2017.07.032.

[23] T. Wang, Q. Han, F. Chu, and Z. Feng. Vibration based condition monitoring and fault diagnosis of wind turbine planetary gearbox: A review. *Mechanical Systems and Signal Processing*, 126:662–685, 2019. doi: 10.1016/j.ymssp.2019.02.051.

[24] S. Schmidt, P.S. Heyns, and K.C. Gryllias. A methodology using the spectral coherence and healthy historical data to perform gearbox fault diagnosis under varying operating conditions. *Applied Acoustics*, 158:107038, 2020. doi: 10.1016/j.apacoust.2019.107038.

[25] Y. Li, K. Feng, X. Liang, and M.J. Zuo. A fault diagnosis method for planetary gearboxes under non-stationary working conditions using improved Vold-Kalman filter and multi-scale sample entropy. *Journal of Sound and Vibration*, 439:271–286, 2019. doi: 10.1016/j.jsv.2018.09.054.

[26] S. Tong, Y. Huang, Y. Jiang, Y. Weng, Z. Tong, N. Tang, and F. Cong. The identification of gearbox vibration using the meshing impacts based demodulation technique. *Journal of Sound and Vibration*, 461:114879, 2019. doi: 10.1016/j.jsv.2019.114879.

[27] X. Chen and Z. Feng. Time-frequency space vector modulus analysis of motor current for planetary gearbox fault diagnosis under variable speed conditions. *Mechanical Systems and Signal Processing*, 121:636–654, 2019. doi: 10.1016/j.ymssp.2018.11.049.

[28] D.F. Plöger, P. Zech, and S. Rinderknecht. Vibration signature analysis of commodity planetary gearboxes. *Mechanical Systems and Signal Processing*, 119:255–265, 2019. doi: 10.1016/j.ymssp.2018.09.014.

[29] G. D'Elia, E. Mucchi, and M. Cocconcelli. On the identification of the angular position of gears for the diagnostics of planetary gearboxes. *Mechanical Systems and Signal Processing*, 83:305–320, 2017. doi: 10.1016/j.ymssp.2016.06.016.

[30] W. Żurowski, K. Olejarczyk, and R. Zaręba. Wear assessment of sliding sleeves in a single-stage cycloidal drive. *Advances in Science and Technology Research Journal*, 13(4):239–245, 2019. doi: 10.12913/22998624/114180.

[31] K. Olejarczyk, M. Wikło, K. Kołodziejczyk, R. Król, and K. Król. Theoretical and experimental verification of one stage cycloidal gearbox efficiency. In: T. Uhl (ed.) *Advances in Mechanism and Machine Science. Proceedings of the 15th IFToMM World Congress on Mechanism and Machine Science*, pages 1029–1038, Cracow, Poland, 15-18 July, 2019. doi: 10.1007/978-3-030-20131-9_102.

[32] M. Wikło, K. Olejarczyk, K. Kołodziejczyk, K. Król, and I. Komorska. Experimental vibration test of the cycloidal gearbox with different working conditions. *Vibroengineering PROCEDIA*, 13:24–27, 2017. doi: 10.21595/vp.2017.19073.